A Non-isothermal Pore Network drying Model: Influence of Gravity
Proceedings of European Congress of Chemical Engineering (ECCE-6)
Copenhagen, 16-20 September 2007

A Non-isothermal Pore Network Drying Model: Influence of Gravity

V. K. Surasani, T. Metzger, E. Tsotsas

Institute of Process Engineering, Chair of Thermal Process Engineering,
Otto-von-Guericke-University Magdeburg, P. O: 4120, D-39016 Magdeburg, Germany

Abstract

The concept of immiscible displacement as an invasion percolation (IP) process driven by heat and mass transfer is used in a pore network model for convective drying of capillary porous media. The coupling between heat and mass transfer occurs at the liquid-gas interface through temperature dependent equilibrium vapour pressure, surface tension and phase change enthalpy (in evaporation and condensation). The interfacial effects due to capillary forces and gravity are combined in an invasion potential Φ; viscous forces are neglected. Simulation results show stabilized invasion patterns and finite drying front width by the influence of gravity.

Keywords: capillary porous media, mono-modal pore size distribution, invasion percolation, phase distributions, temperature field

1. Introduction

The fundamental understanding of pore network modelling commences with the representation of the void space, i.e. geometry, in the porous medium. Most of the cases in literature have adopted the network representation of void space in the form of sites (pores) connected with bonds (throats) [1, 2]. In the present work, void space in the porous medium is regarded as a network of cylindrical throats with randomly distributed radius and connections are by pores. Figure 1 shows the network of pores and throats in a two-dimensional square lattice and how each pore is associated with a control volume. Further, drying can be treated as a special case of invasion percolation (IP) [3] due to the immiscible displacements of air and liquid in the pore space upon evaporation of liquid. During this invasion process, liquid menisci will respond to capillary, viscous and buoyancy forces. In the absence of viscous forces, gravity and thermal gradients, phase distributions completely depend on the spatial disorder of pore size [4]. In the presence of gravity, the phase distributions are patterns of invasion percolation in a stabilizing gradient (IPSG) or in a destabilizing gradient (IPDG) depending on the direction of the gravity vector to the main direction of vapour flow [4]. Similarly, IPSG patterns can be observed in the presence of viscous forces [1, 5].

In the above-mentioned literature, invasion is considered at slow drying rates; energy aspects of the drying are neglected when studying the physical and structural influences on invasion patterns. The influence of temperature gradients – which were imposed onto the drying product – has been investigated by Plourde and Prat [6], Huinink et al. [7]. However, product temperature did not evolve freely as corresponding to convective drying boundary conditions. Surasani et al. [8] considered heat transfer in a pore network model that neglects viscous effects and gravity. Consequently, the model is the first to describe the free evolution of temperature fields in convective drying. The model assumes dominant capillary forces and neglects both viscous forces and gravity.

The present work extends this first model to investigate the interplay between capillary and gravitational forces (still neglecting viscous effects) as occurring in convective heating. The throat invasion order is then determined by an invasion potential Φ, which combines both effects of capillarity and gravity. The assumption of quasi-stationary vapour transport under constant total pressure is applied. Heat transfer is due to conduction and local thermal equilibrium is assumed in each control volume. In this way, gravitational stabilization of the drying front is superimposed by thermal stabilization. Simulation results are shown as drying curves, temporal evolution of phase distributions (cluster formation), temperature fields and phase diagrams for a mono-modal pore size distribution.

2. Modelling

Initially, the network is saturated completely with water at room temperature T_{in} (= 20°C) and drying air flows at zero humidity ($P_{v,\infty} = 0$) and temperature T_∞ over the top edge of the network. To describe the first drying period with its constant drying rate, it is necessary to model the convective boundary layer in a discretized way, by extending the network into the gas-phase with additional nodes (see Figure 1); their number is given by mass transfer coefficient and vapour diffusivity [9]. Immiscible displacements upon evaporation of liquid will cause the different invasion percolation gradient (IPG) patterns in the network. One such pattern is shown in Figure 1 which represents the continuous vapour phase and disconnected liquid clusters in the solid network. Pore and throat conditions [8] will determine the transport within and between the phases. At the phase boundary liquid flow, evaporation and vapour

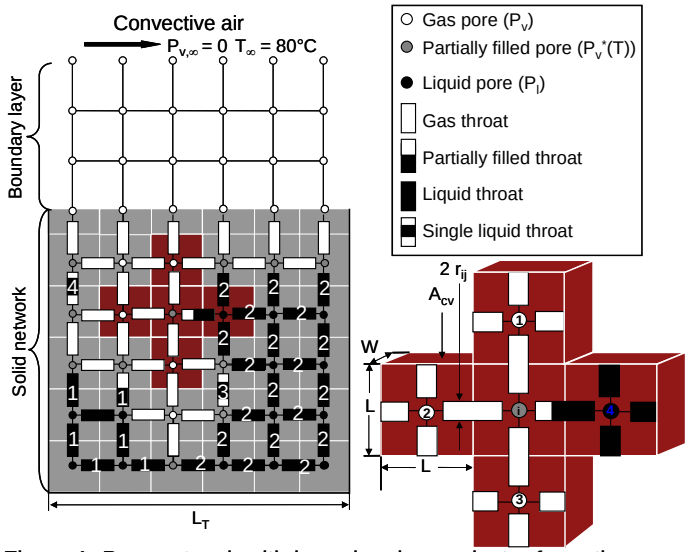

Figure 1: Pore network with boundary layer, cluster formations, pore and throat conditions and control volume i .

diffusion are simultaneous. In partially filled throats, the meniscus moves as evaporated vapour diffuses through air and, at the same time, liquid flows in either direction depending upon boundary liquid pressure at meniscus. Pore saturations are given by average throat saturations of connected throats. Equilibrium vapour pressure exists in partially filled pores, which give boundary conditions to the linear system of vapour transport. The other kind of boundaries comes from convective air partial vapour pressure ($P_{v,\infty}$ =0).

2.1 Vapour transport

The vapour flow rate between two gas pores is given by Stefan's law. From the law of conservation and the assumption of quasi-stationary vapour transport, total mass flow rates ($\dot{M}_{v,ij}$) from any gas pore is equal to zero.

$$\sum_{j=1}^{4}\dot{M}_{v,ij}=\sum_{j=1}^{4}A_{ij}\frac{\delta}{L}\frac{P\tilde{M}_v}{\tilde{R}T}\ln\left(\frac{P-P_{v,i}}{P-P_{v,j}}\right)=0 \qquad (1)$$

Here cross sectional area varies from the solid network ($A_{ij}=\pi r_{ij}^2$) to the boundary layer (A_{ij} = LW). Since we neglect the overlap of throats at pore nodes, all throats in the network are assumed as equal in length (L_{ij} = L). The linear system of vapour transport Eq. (1) is solved for partial vapour pressures ($P_{v,i}$) using the conjugate gradient method (CGM).

2.2 Liquid transport

The assumption of negligible viscous forces implies that, in each cluster, liquid can be pumped from the throat with the highest liquid pressure to all other meniscus throats, making them moving meniscus (MM) throats and stationary meniscus (SM) throats, respectively. In each cluster, the MM throat will empty first since this throat alone will contribute to the total evaporation of the cluster through capillary pumping. The criterion for selecting MM throats is given by throat potential ($P_{l,ij}$ = P + Φ_{ij}), i.e. in each cluster, the throat with highest invasion potential Φ is selected as MM throat. So, it is necessary to identify the continuous liquid phases, i.e. clusters, and within each cluster the highest invasion

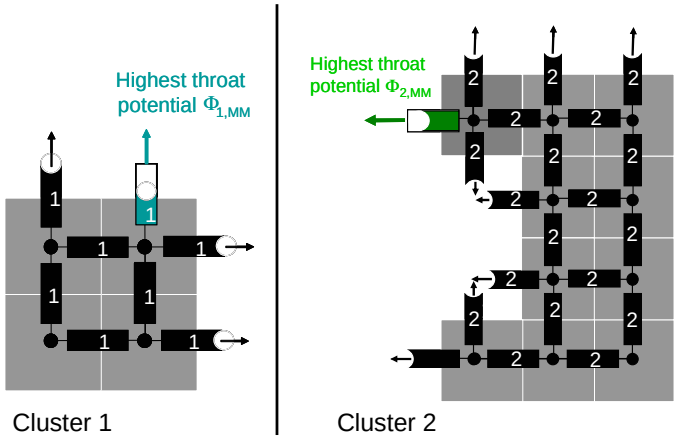

Figure 2: Highest invasion potential throats for the two clusters of Fig. 1.

potential $\Phi_{nc,MM}$ throat. To this purpose, the Hoshen-Kopelman algorithm (well documented in literature) can be used [10, 11] for cluster labelling and invasion potential is given by combined capillary force and gravity as

$$\Phi = \frac{-2\sigma(T_{ij})}{r_{ij}} + (\rho_l - \rho_g)\, g\, h_{ij} \tag{2}$$

Figure 2 shows the realization for the clusters 1 and 2 of Fig. 1. The time step Δt to empty the MM throat in each cluster (nc) can be obtained from the ratio of current mass in the MM throat to the total evaporation rate of the cluster as

$$\Delta t_{m,nc} = \frac{\rho_l V_{MM,nc}}{\sum_{j=1}^{mt} \dot{M}_{ev,ij,nc}} \tag{3}$$

The minimum time step $\Delta t_{m,min}$ has to be chosen among the existing clusters and single throats for throat invasion.

2.3 Transient heat transfer

Figure 1 also shows how each control volume is represented by one pore and contains four-half throats, i.e. each throat participates in two control volumes. Liquid of partially filled throats are equally distributed to neighbour pores. The transient energy balance equation over the control volume is given by

$$V_i (\rho c_p)_i \frac{dT_i}{dt} = -\sum_{j=1}^{4} A_{cv,ij}\, \lambda_{ij} \frac{T_i - T_j}{L} - \Delta h_{v,i}(T_i) \sum_{j=1}^{lm} \dot{M}_{ev,ij} \tag{4}$$

where $\Delta h_{v,i}(T_i)$ is phase change enthalpy (absolute value). The mass flow rate $\dot{M}_{ev,ij}$ is positive for evaporation and negative for condensation. The meniscus position is used to allocate heat sink/source to a control volume. The exchange area is $A_{cv,ij} = LW$ (because both voids and solid can contribute to heat transfer). The effective thermal conductivities λ_{ij} and control volume heat capacities $V_i (\rho c_p)_i$ are functions of throat saturation [8]. The stability of the explicit method is only guaranteed if the thermal time step fulfils the condition.

$$\Delta t_t < \frac{(\rho c_p)_i L^2}{\sum_j \lambda_{ij}} \tag{5}$$

2.4 Drying algorithm

First, the data structures describing the pore grid of network and boundary layer must be formed from network size (e.g. 51×51); additionally, drying air velocity, initial and boundary conditions are set. The linear system for vapour transport (Eq. (1)) is solved and the evaporation rates at each meniscus are computed. Then, from the invasion potential Φ in meniscus throats, the MM throat is identified for each cluster, and the minimal mass transfer time step $\Delta t_{m,min}$ calculated. The time step Δt_{min} is

chosen as the minimum out of mass transfer time step $\Delta t_{m,min}$ and heat transfer time step Δt_t, which obeys stability criteria of Eq. (5). The mass loss due to evaporation is computed for the time step Δt_{min}. Next, the new temperature field is computed by using Eq. (4) for same time step Δt_{min}. Finally, phase distributions (pore and throat saturations) and temperature fields (as well as temperature dependent variables) are updated. The procedure will be repeated until all liquid is removed from the network.

3. Results

The results presented in this section have been obtained for networks of size 51×51 with mono-modal throat size distribution 40 ± 2 μm (see Fig. (4) for realization) and, throat length is 500 μm. Initially, the network is saturated with water and has a uniform temperature of 20°C. The heat transfer parameters of the solid are chosen as for glass: $(\rho c_p)_s = 1.7 \cdot 10^6$ J/(m^3 K) and $\lambda_s = 1$ W/(m K). Bulk air is at $T_\infty = 80$°C, has zero moisture content and velocity such that the boundary layer contains 7 nodes (β = 7.3 mm/s). Simulations of convective heating mode with and without gravity are presented.

Figure 3 shows the drying kinetics for the mono-modal pore network as network saturation versus time. The temporal evolutions of phase distributions (IP patterns) and temperature fields are shown in Fig. 4; the respective overall network saturations are indicated for simulations of both without and with gravity. At the start of the drying process both curves in Fig. 3 shows similar drying rates (from the slope). The similar IP patterns can be seen at network saturation S equal to 0.95 (Fig. 4) since capillary forces are dominant over gravity in selecting the highest invasion potential throat. In both cases, drying rate falls drastically due to the increase in resistance to vapour diffusion during the emptying of surface throats. Further, drying rates are lower in the case of gravity and longer drying times are observed.

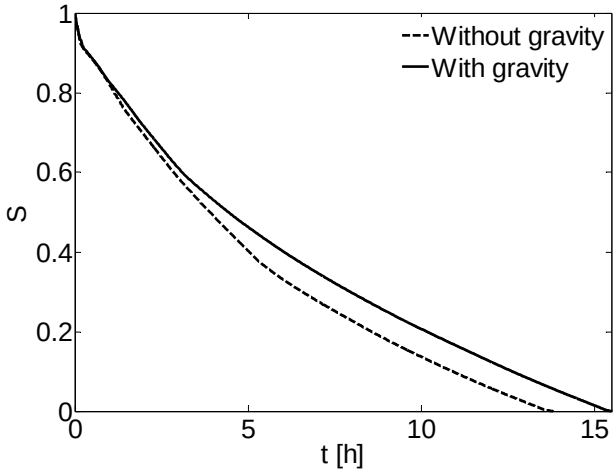

Figure 3: Overall saturation of the network versus time

In absence of gravity, i.e. with Bond number B = 0, capillary forces alone will determine the order of throat invasion; they are given by random throat radius distribution and current local temperatures (Eq. (2)). If temperature gradients are low, then the gas phase will rapidly invade the depth of the pore network creating many liquid clusters in the whole network. This results in IP patterns without significant stabilization as shown in Fig. 4 (case without gravity). For the given geometry, gravity counteracts capillary forces. Throat invasion order is then determined by invasion potential Φ, which combines both capillary force and gravity. The drying

front is limited to finite width and recedes into the network with out any major changes. This phenomenon of invasion percolation in a stabilizing gradient (IPSG) is shown as phase patterns in Fig. 4 (with gravity). The observed drying rates are low in the case of gravity (see Fig. 3 with gravity) because of the increased resistance to vapour diffusion for a stabilized front. Capillary pumping is limited to a finite drying front in which small clusters will form (see Fig. 4 with gravity).

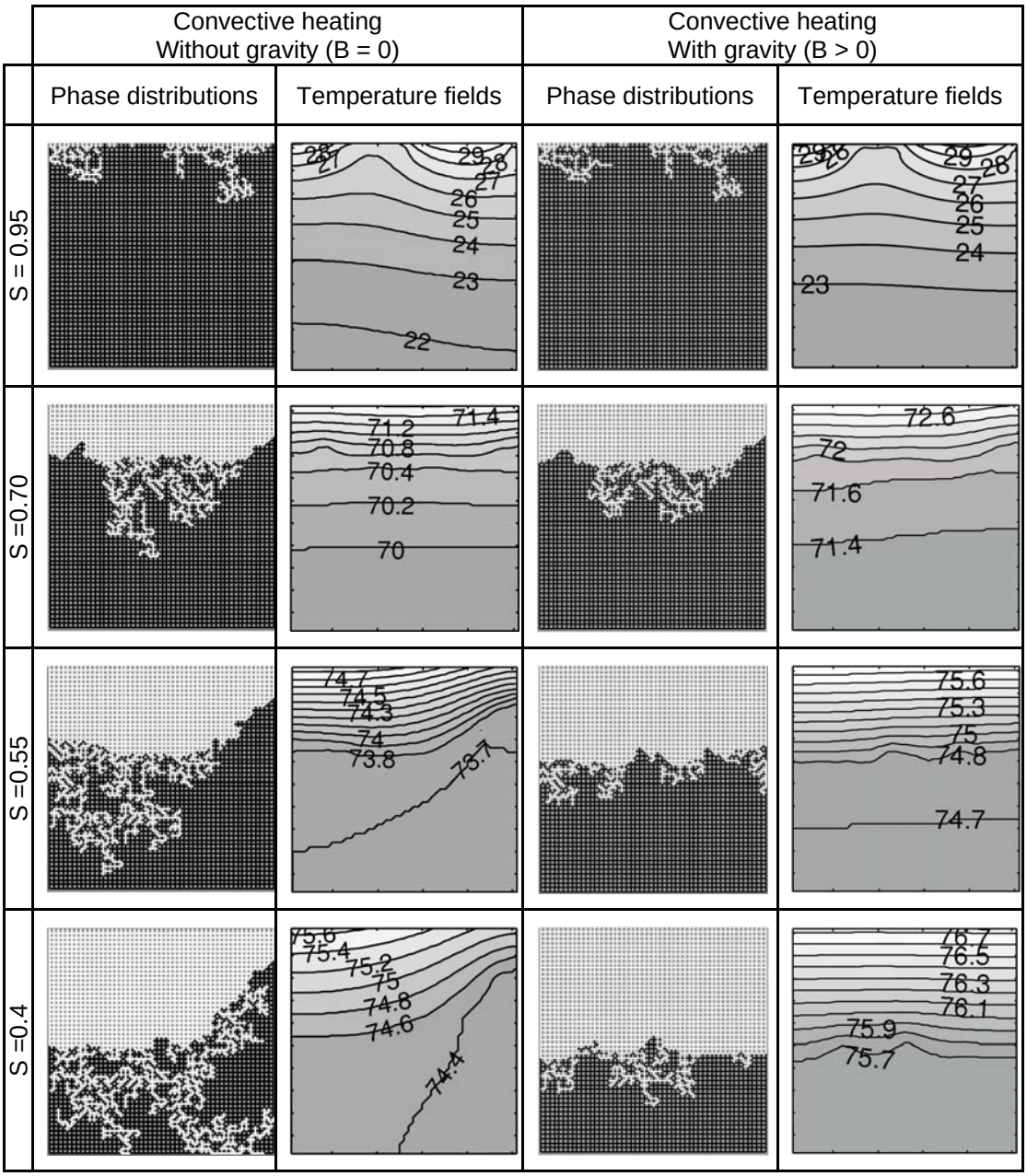

Figure 4: Comparison of evolved phase distributions and temperature fields without and with gravity.

Figure 5 represents the phase diagrams of mono-modal network for both cases of without and with gravity. The phase evolutions are plotted in terms of dimensionless

length versus total network saturation S. The regions of evolved phases, i.e. gas, liquid and liquid-gas interface, are named in the figure. The upper boundary in the liquid-gas interface indicates the dimensionless length above that only gas phase exists. Above this boundary, only vapour diffusion takes place. One can see the main cluster disconnection point (MCD) in both figures. MCD indicates the point where all the surface throats dry out and the surface losses contact with main liquid cluster. At this point, the overall drying rates will fall down drastically. The lower boundary of liquid-gas interface indicates the dimensionless length below which only liquid phase exists. Only liquid flow due to capillary pumping will takes place in this region. The point at which air invades the bottom of the network, i.e. where liquid-gas interface lower boundary reaches the bottom of the network, is called breakthrough point (BT). Invasion percolation in a stabilizing gradient is characterized by the magnitude of liquid-gas interface. At the start of the drying process, both cases of without and with gravity represent same magnitude of liquid-gas interface and similar invasion patterns; and also similar main cluster disconnection (MCD) points are observed. In the absence of gravity, the magnitude of liquid-gas interface increases while the upper boundary stays constant and results in an earlier BT point. This characterizes unstabilized invasion percolation patterns.

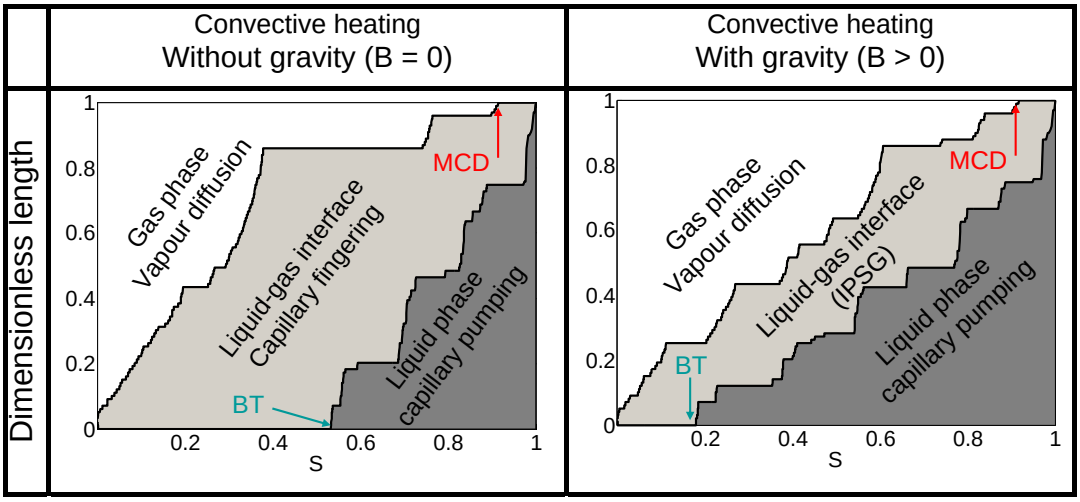

Figure 5: Phase evolutions of the network interns of dimensionless network length and over all saturation of the network.

In the presence of gravity, liquid-gas interface is of almost constant magnitude characterizing IPSG patterns. In both cases, after BT point liquid-gas interface diminishes as upper boundary recedes to the bottom of the network.

4. Conclusions

A non-isothermal pore network drying model including gravity and capillary forces is presented which shows invasion percolation stabilizing gradient (IPSG) patterns. In the presence of gravity, IP patterns completely depend on the invasion potential Φ, i.e. the net pressure due to combined capillary forces and gravity. In convective drying, the porous medium heats up from the surface; this leads to favourable

invasion of near surface throats (influence of temperature dependent surface tension in Φ). This thermal stabilization becomes important for weakly disordered networks [8]. The above-mentioned thermal stabilization of the drying front is now superimposed by a gravitational stabilization. However, the evolved temperature gradients over the network are small and play a minor role on IP patterns in the presented case. Unstabilized invasion percolation patterns with large drying front width, without gravity, and invasion percolation stabilizing gradient (IPSG) patterns with finite drying front width, with gravity, are shown as the result of simulations on a mono-modal pore network. The characteristic liquid-gas interface is presented for both with and without gravity in the form of phase diagram. For the gravity-controlled case, the evolved constant magnitude of liquid-gas interface indicates the finite drying front width in which very few cluster will form. The observed drying rates are low due to the increase in the resistance to vapour diffusion in the presence of a stabilized drying front.

Future work will include the investigation of combined influence of all forces acting on the menisci. This needs the necessity of including viscous forces in the liquid flow. Furthermore, model needs to be extended for three-dimensional networks since the invasion patterns are significantly different in this case. To this purpose, the drying algorithm needs to be improved to reduce high computational time.

Acknowledgement

This work was financed by the German Research Foundation (DFG) in the frame of Graduate School 828 “Micro-Macro-Interactions in Structured Media and Particle Systems”. The first author would like to express his special thanks to Max-Buchner-Forschungsstiftung for its additional support.

Nomenclature

A	area of cross section (m^2)
c_p	specific heat capacity (J/kg/K)
g	mass transfer conductance (kg/s)
L	length of throat (m)
$\tilde{M}$	molar mass (kg/kmol)
$\dot{M}$	mass flow rate (kg/s)
N	number of pores/clusters (–)
P	pressure (Pa)
$\dot{Q}$	heat flow rate (W)
$\tilde{R}$	ideal gas constant (J/kmol/K)
r	throat radius (m)
S	saturation (–)
T	temperature (K)
t	time(h)
V	volume (m^3)
W	network thickness (m)
Δh	specific phase change enthalpy (J/kg)

Greek Symbols

α	heat transfer coefficient ($W/m^2/K$)
γ	surface tension (N/m)
δ	vapour diffusivity (m^2/s)
λ	thermal conductivity (W/m/K)
ρ	density (kg/m^3)

Subscripts/ Superscripts

c	capillary
ev	evaporation

g	gas	nc	cluster number
i or j	pore or node	s	solid
ij	throat connecting pores i and j	v	vapour
l	liquid	*	equilibrium
lm	number of menisci		

References

[1] A. G. Yiotis, A. K. Stubos, A. G. Boudouvis and Y. C. Yortsos, Advances in Water Resources 24, 439-460, 2001.

[2] S. C. Nowicki, H. T. Davis and L. E. Scriven, Drying Technology 10(4), 925-946, 1992.

[3] M. Prat, International Journal of Multiphase flow 21(5), 875-892, 1995.

[4] J. B. Laurindo, and M. Prat, Chemical Engineering Science 53, 2257-2269, 1998.

[5] T. Metzger, A. Irawan, and E. Tsotsas, Drying Technology 25, 49-57, 2007.

[6] F. Plourde and M. Prat, International Journal of Heat and Mass Transfer 46, 1293-1307, 2003.

[7] H. Huinink, L. Pel, M. A. J. Michels. and M. Prat, The European Physical Journal E 9, 487-498, 2002

[8] V. K. Surasani, T. Metzger and E. Tsotsas, Consideration of heat transfer in pore network modelling of convective drying, Accepted in International. Journal of Heat and Mass Transfer.

[9] T. Metzger, A. Irawan and E. Tsotsas, Proceedings of 3rd Nordic Drying Conference, Karlstad, Sweden, 15-17 June 2005

[10] A. Al-Futaisi and T. W. Patzek, Physica A 321, 665-678, 2003.

[11] T. Metzger, A. Irawan and E. Tsotsas, Physica A, 321(2003), 665-678, Physica A 363 558-560, 2006.